




Myocardial perfusion assessment in the infarct core and penumbra zones in an in-vivo porcine model of the acute, sub-acute, and chronic infarction

Meng-xi Yang¹ · Hua-yan Xu² · Lu Zhang² · Lin Chen² · Rong Xu² · Hang Fu² · Hui Liu² · Xue-sheng Li³ · Chuan Fu³ · Ke-ling Liu⁴ · Hong Li⁵ · Xiao-yue Zhou⁶ · Ying-kun Guo² · Zhi-gang Yang^{1,4} 

Received: 28 December 2019 / Revised: 12 July 2020 / Accepted: 21 August 2020 / Published online: 6 November 2020
© European Society of Radiology 2020

Abstract

Objectives To assess the longitudinal changes of microvascular function in different myocardial regions after myocardial infarction (MI) using myocardial blood flow derived by dynamic CT perfusion (CTP-MBF), and compare CTP-MBF with the results of cardiac magnetic resonance (CMR) and histopathology.

Methods The CTP scanning was performed in a MI porcine model 1 day ($n = 15$), 7 days ($n = 10$), and 3 months ($n = 5$) following induction surgery. CTP-MBF was measured in the infarcted myocardium, penumbra, and remote myocardium, respectively. CMR perfusion and histopathology were performed for validation.

Results From baseline to follow-up scans, CTP-MBF presented a stepwise increase in the infarcted myocardium (68.51 ± 11.04 vs. 86.73 ± 13.32 vs. 109.53 ± 26.64 ml/100 ml/min, $p = 0.001$) and the penumbra (104.92 ± 29.29 vs. 120.32 ± 24.74 vs. 183.01 ± 57.98 ml/100 ml/min, $p = 0.008$), but not in the remote myocardium (150.05 ± 35.70 vs. 166.66 ± 38.17 vs. 195.36 ± 49.64 ml/100 ml/min, $p = 0.120$). The CTP-MBF correlated with max slope ($r = 0.584$, $p < 0.001$), max signal intensity ($r = 0.357$, $p < 0.001$), and time to max ($r = -0.378$, $p < 0.001$) by CMR perfusion. Moreover, CTP-MBF defined the infarcted myocardium on triphenyl tetrazolium chloride staining (AUC: 0.810, $p < 0.001$) and correlated with microvascular density on CD31 staining ($r = 0.561$, $p = 0.002$).

Conclusion CTP-MBF could quantify the longitudinal changes of microvascular function in different regions of the post-MI myocardium, which demonstrates good agreement with contemporary CMR and histopathological findings.

Key Points

- The CT perfusion-based myocardial blood flow (CTP-MBF) could quantify the microvascular impairment in different myocardial regions after myocardial infarction (MI) and track its recovery over time.
- The assessment of CTP-MBF is in good agreement with contemporary cardiac MRI and histopathological findings, which potentially facilitates a rapid approach for pathophysiological insights following MI.

Meng-xi Yang and Hua-yan Xu contributed equally to this work and should be considered as the equal first authors.

Supplementary Information The online version of this article (<https://doi.org/10.1007/s00330-020-07220-x>) contains supplementary material, which is available to authorized users.

✉ Zhi-gang Yang
yangzg666@163.com

Ying-kun Guo
gykpanda@163.com

¹ Department of Radiology, State Key Laboratory of Biotherapy and Cancer Center, West China Hospital, Sichuan University, Chengdu, China

² Department of Radiology, Key Laboratory of Obstetric & Gynecologic and Pediatric Diseases and Birth Defects of Ministry of Education, West China Second Hospital, Sichuan University, Chengdu, China

³ Department of Radiology, West China Second Hospital, Sichuan University, Chengdu, China

⁴ Department of Radiology, West China Hospital, Sichuan University, Chengdu, China

⁵ Key Laboratory of Birth Defects and Related Diseases of Women and Children of Ministry of Education, West China Second Hospital, Sichuan University, Chengdu, China

⁶ MR Collaboration, Siemens Healthcare Ltd, Shanghai, China

Keywords Myocardial infarction · Microcirculation · Tomography, X-ray computed · Magnetic resonance imaging

Abbreviations

CAD	Coronary artery disease
CMR	Cardiac magnetic resonance
CTA	CT angiography
CTP	CT perfusion
H&E	Hematoxylin-eosin
LGE	Late gadolinium enhancement
MBF	Myocardial blood flow
MI	Myocardial infarction
ROI	Region of interest
SI	Signal intensity
SPECT	Single-photon emission computed tomography
TTC	Triphenyl tetrazolium chloride
TTM	Time to maximum signal intensity

Introduction

Following myocardial infarction (MI), microvascular impairment is associated with poor long-term recovery and outcomes [1, 2]. Therefore, it is vital to assess microvascular function to identify the risk stratification and subsequent intervention efficiency [3, 4]. Currently, single-photon emission computed tomography (SPECT), positron emission tomography, and cardiac magnetic resonance (CMR) comprise the conventional modalities for myocardial perfusion assessment [3–7]. However, CT perfusion (CTP) has been recently proposed as an alternative imaging modality [8, 9]. Compared with other imaging modalities, CTP offers the distinct advantages of fast acquisition speed and high patient acceptability, and it is especially suitable for patients who are incapable of undergoing long-term examinations [10, 11]. It should also be mentioned that the combination of CT angiography (CTA) and CTP allows simultaneous evaluation of coronary artery anatomy and myocardial perfusion in a one-shot examination [8, 12].

Extensively applied in the diagnosis of coronary artery disease (CAD), CTP provides a high diagnostic accuracy for myocardial ischemia and adds incremental prognostic value over CTA [5, 12–15]. Moreover, the myocardial blood flow derived by dynamic CTP (CTP-MBF) potentially allows the quantitative assessment of microvascular dysfunction [8, 9]. Previous published study demonstrated that CTP-MBF could efficiently detect perfusion abnormalities in patients with suspected CAD and further differentiate myocardial infarction from myocardial ischemia [16]. These findings suggest that CTP-MBF may be a potential biomarker for myocardial viability following MI that can reflect microvascular impairment severity, thus benefiting to the individual cardioprotective management.

Therefore, this study sought to investigate (1) the microvascular function of different regions of the post-MI

myocardium over time by CTP-MBF and (2) the correlation of CTP-MBF with contemporary CMR and histological findings in a MI porcine model.

Methods

Animal preparation

The animal protocols were approved by the Institutional Animal Care and Use Committee of our hospital. A total of 18 Bama miniature pigs were used in this experiment. While preparing for the operation, the animals were placed under anesthesia and their venous channels were established via an ear vein. The electrocardiogram, heart rate, blood pressure, and blood oxygen saturation data were monitored throughout the surgery. MI was induced by ligating the left anterior descending artery via thoracotomy and was subsequently confirmed by the elevation of ST segment on the electrocardiogram [17]. Three pigs died because of arrhythmia during the surgery, despite resuscitation efforts.

Imaging scans were serially performed in the surviving pigs 1 day (acute scan, $n = 15$), 7 days (sub-acute scan, $n = 10$), and 3 months (chronic scan, $n = 5$) following the surgery, respectively. CMR was performed before CTP and the interval between CMR and CTP scans was within 2 h.

Dynamic CT image acquisition

CTP examinations were performed using a Revolution CT Scanner (GE Healthcare), in combination with a 16-cm-wide coverage, 0.23-mm spatial resolution, 0.28-s gantry rotation time, intracycle motion-correction algorithm, and last-generation iterative reconstruction. The scanning parameters were as follows: tube voltage, 80 kV; tube current, 199 mA; slice thickness, 1.25 mm; R-R interval, 45%. The iodinated contrast agent (2 ml/kg, 2 ml/s flow [iopamidol, 370 mg iodine/ml, Bayer Yakuhin, Ltd.]) was infused with electrocardiogram monitoring (Stellant Dual Flow) and followed by 10 ml saline solution chaser at a rate of 2 ml/s. Prior to the CTP examination, a test bolus of 5-ml contrast agent was acquired as a baseline to calculate the acquisition delay for CTP [18].

CMR image acquisition

The CMR examinations were performed using a 3.0-T MR scanner (MAGNETOM Skyra, Siemens) with an 18-channel body coil combined with a spine coil (12 of 36 channels used). The CMR protocol included cardiac cine, first-pass perfusion, and late gadolinium enhancement (LGE) imaging. All images were

acquired under electrocardiograph gating. Cine imaging used a balanced steady-state free-precession pulse sequence (echo time (TE) = 1.48 msec; repetition time (TR) = 43.94 msec; flip angle = 46°; slice thickness 5 mm; matrix = 142 × 142 pixels; field of view (FOV) = 213 × 213 mm²). For perfusion imaging, a dose of 0.2 ml/kg gadobenate dimeglumine (MultiHance) was administered using an automated injector (Stellant, MEDRAD) at a flow rate of 2 ml/s, followed by a 10 ml saline flush at a rate of 2 ml/s. The perfusion images were acquired in three standard short-axis slices (apical, middle, and basal) and in one slice of the 4-chamber view using an inversion-recovery prepared echoplanar imaging sequence (TE = 1.26 msec; TR = 287.48 msec; flip angle = 10°; matrix = 123 × 123; slice thickness = 6 mm; FOV = 160 mm × 160 mm). Each set of first-pass perfusion images was completed in 80 cardiac cycles. LGE image was acquired 15 min post-contrast (TE = 1.24 msec; TR = 456 msec; flip angle = 55°; slice thickness = 6 mm; matrix = 262 × 262 pixels; FOV = 340 × 234 mm).

Image analysis

The images were analyzed by two radiologists who had a minimum of 3 years' experience. The CMR image analysis was performed using the image software (Cvi42; Circle Cardiovascular Imaging, Inc.). The infarcted myocardium was defined as five SD above the mean intensity of normal myocardium reference on LGE [19, 20]. The left ventricular functional parameters following ligation were analyzed as previously described [21]. The CMR perfusion quantitative parameters including max slope, max signal intensity (max SI), and time to maximum signal intensity (TTM) were obtained from the myocardial signal intensity-time curve [22]. Two types of analysis were conducted on one short-axis slice with the largest infarct size of each animal. To measure the perfusion parameters of different regions of the post-MI myocardium, the region of interest (ROI) measurement was manually drawn in the infarcted zone (five SD above mean intensity of normal myocardium on LGE) [4, 20, 23], penumbra (the myocardium adjacent to infarcted zone) [24, 25], and remote myocardium (the myocardium 180° from the infarcted zone). To reflect the severity of myocardial injury following MI, the segmental measurement of infarct transmuralities on LGE and the CMR perfusion parameters were calculated by dividing the myocardium into six distinct segments. According to the LGE images, the segments with enhanced myocardium (infarcted myocardium) were defined as infarcted segments, while those without enhanced myocardium were defined as non-infarcted segments [16].

The acquired CTP images were then analyzed at the image processing workstation (Ziostation2). The CTP-MBF color image of the myocardium was calculated using the maximum slope method. The ROI-based and segment-based CTP-MBF was then measured on short-axis images and subsequently correlated with MR image analysis. Images containing

artifacts which undermined the reliable assessment were excluded both in CMR and CT analysis.

Histology and immunohistochemistry

Following imaging scans, randomized euthanasia was immediately performed using potassium chloride in pigs at 1 day ($n = 5$), 7 days ($n = 5$), and 3 months ($n = 5$) following MI. The euthanasia of animals was performed without knowing the imaging findings in order to avoid any selection bias. The extracted hearts were rinsed in the saline solution and then cut into 6-mm slices, with each slice corresponding to the short-axis images of CMR and CTP.

For triphenyl tetrazolium chloride (TTC) staining, the slices were submerged in 2% 2,3,5-TTC solution (Sigma, T8877) for 15 min in a warm bath at 37 °C, to determine myocardial viability. The TTC-stained heart tissues were then put onto a blue sheet of paper and photographed with a digital camera. The slices were then divided into six segments according to the segment-based image analysis. The segments that had poorly stained myocardium (infarcted myocardium) were defined as the infarcted segments [17]. The infarct transmuralities per segment were measured using Image-Pro Plus 6.0 software (Media Cybernetics).

For microscopical examination of the myocardium, the slices were fixed in 10% formalin and processed by dehydrating the tissue in increasing concentrations of ethanol. Samples were then cleared in xylene, embedded in paraffin wax, and cut into 5- μ m sections. For histopathological analysis, sections were stained with hematoxylin and eosin (H&E) (Servicebio, G1005). For immunohistochemical analysis, the sections were deparaffinized and antigen unmasking was performed with citrate buffer at pH 6. Before incubation with primary antibodies, endogenous peroxidase was blocked by incubation with H₂O₂ for 5 min and endogenous antigens were blocked with normal rabbit serum for 30 min. The primary antibodies were anti-CD31 (Abcam, Ab28364) as it could detect microvessels. Bound antibody was revealed by staining with diaminobenzidine (Servicebio, G1211) and nuclei were counterstained with hematoxylin (Servicebio, G1004). The histologic results were observed at a high-power lens (magnification, × 200) using a microscope (Leica, DMI4000B). The microvascular density of infarcted myocardium, penumbra, and remote myocardium was measured in the corresponding area on immunoreactive CD31 staining [26, 27].

Statistical analysis

Data were analyzed using the SPSS software for Windows (version 23.0; SPSS Inc.). Categorical or enumeration data were expressed as numbers (percentages). As for continuous variables, the normally distributed parameters were expressed as the mean ± standard deviation, whereas the non-normally distributed parameters were expressed as the median

(interquartile range). Furthermore, the comparison of CTP-MBF of different myocardial regions in different settings was tested by the analysis of variance. Bivariate correlations were analyzed using Pearson’s or Spearman’s method, as appropriate. ROC analysis was used to test the diagnostic performance of CTP-MBF to differentiate between the infarcted segments and the non-infarcted segments, which were confirmed by LGE and TTC staining, respectively. Finally, the inter- and intra-observer variability of CTP-MBF measurements were tested by the intraclass correlation coefficient. All tests were 2-tailed, and *p* values < 0.05 were considered significant.

Results

Baseline characteristics of experimental animals

A total of 15 pigs survived the surgery. Consequently, CTP and CMR were performed in the acute (1 day after MI), sub-acute (7 days after MI), and chronic (3 months after MI) settings. For the histological examination, the pigs were immediately euthanized following acute (*n* = 5/15, 33.33%), sub-acute (*n* = 5/10, 50%), and chronic (*n* = 5/5, 100%) scans. The baseline characteristics of the pigs are described in Table 1 and the imaging indexes are summarized in Table 2. The variation of myocardial perfusion is shown in Fig. 1 and Fig. S1.

Longitudinal changes of CTP-MBF in different regions following MI

There was a stepwise increase in CTP-MBF among infarcted myocardium, penumbra, and remote myocardium in acute

settings (68.51 ± 11.04 vs. 104.92 ± 29.29 vs. 150.05 ± 35.70 ml/100 ml/min, *p* < 0.001). A similar trend was also identified in the sub-acute setting (86.73 ± 13.32 vs. 120.32 ± 24.74 vs. 166.66 ± 38.17 ml/100 ml/min, *p* < 0.001). On the other hand, there was an increase of CTP-MBF in the chronic setting in infarcted myocardium (68.51 ± 11.04 vs. 86.73 ± 13.32 vs. 109.53 ± 26.64 ml/100 ml/min, *p* = 0.001) and penumbra (104.92 ± 29.29 vs. 120.32 ± 24.74 vs. 183.01 ± 57.98 ml/100 ml/min, *p* = 0.008), but not in remote myocardium (150.05 ± 35.70 vs. 166.66 ± 38.17 vs. 195.36 ± 49.64 ml/100 ml/min, *p* = 0.120). However, the improvement in the penumbra was significantly more pronounced compared with that in the infarcted one (Fig. 1).

Comparison between CTP-MBF and CMR indexes

The CTP-MBF color map and CMR images of one exemplar case are shown in Fig. 2. A ROI analysis was performed in 15 pigs with acute MI (ROI = 15*3), 10 with sub-acute MI (ROI = 10*3), and five with chronic MI (ROI = 5*3). ROI-based CTP-MBF provided best associations with the max slope (acute setting: *r* = 0.787, *p* < 0.001; sub-acute setting: *r* = 0.741, *p* < 0.001; chronic setting: *r* = 0.848, *p* < 0.001; all settings: *r* = 0.784, *p* < 0.001). CTP-MBF also correlated with max SI (acute setting: *r* = 0.541, *p* < 0.001; sub-acute setting: *r* = 0.648, *p* < 0.001; chronic setting: *r* = 0.796, *p* = 0.003; all settings: *r* = 0.564, *p* < 0.001) and TTM (acute setting: *r* = - 0.464, *p* = 0.001; sub-acute setting: *r* = - 0.412, *p* = 0.024; chronic setting: *r* = - 0.604, *p* = 0.017; all settings: *r* = - 0.417, *p* < 0.001) (Table 3).

A total of 90 myocardial segments in acute setting, 58 segments in sub-acute setting (two segments were excluded for artifacts), and 30 segments in chronic setting were

Table 1 The baseline characteristics of animals

	Acute setting (<i>n</i> = 15)	Sub-acute setting (<i>n</i> = 10)	Chronic setting (<i>n</i> = 5)
Weight, kg	7.70 ± 1.74	6.96 ± 1.23	19.78 ± 3.57
Heart rate, bmp	104.85 ± 30.84	115.89 ± 17.34	124.15 ± 8.90
Post-MI, days	1 (0 to 1)	7 (6 to 8.5)	95 (84 to 97)
Histology examination, <i>n</i> (%)	5 (33.33%)	5 (50%)	5 (100%)
LV function based on CMR			
LVEDV, ml/m ²	16.28 ± 5.12	13.27 ± 2.47	25.73 ± 6.85
LVESV, ml/m ²	10.09 ± 3.00	8.53 ± 2.30	11.22 ± 4.20
LVSV, ml/m ²	6.18 ± 2.77	4.75 ± 1.42	14.52 ± 3.20
LVEF, %	36.98 ± 10.04	35.94 ± 9.86	57.46 ± 8.53
CT radiation dose			
CTDvol, mGy	18.46 ± 1.27	18.41 ± 0.96	18.12 ± 0.47
DLP, mGy cm	221.52 ± 15.23	220.92 ± 11.56	217.42 ± 5.64
ED, mSv	3.10 ± 0.21	3.09 ± 0.16	3.04 ± 0.08

MI, myocardial infarction; CMR, cardiac magnetic resonance; LV, left ventricular; LVEDV, left ventricular end-diastolic volume; LVESV, left ventricular end-systolic volume; LVSV, left ventricular stroke volume; LVEF, left ventricular ejection fraction; CTDvol, volume CT dose index; DLP, dose length product; ED, effective dose

Table 2 The indexes of CTP and CMR

	Acute setting	Sub-acute setting	Chronic setting
CTP indexes			
MBF _{infarct} , ml/100 ml/min	68.51 ± 11.04	86.73 ± 13.32*	109.53 ± 26.64* ^{&}
MBF _{penumbra} , ml/100 ml/min	104.92 ± 29.29	120.32 ± 24.74	183.01 ± 57.98* ^{&}
MBF _{remote} , ml/100 ml/min	150.05 ± 35.70	166.66 ± 38.17	195.36 ± 49.64
CMR perfusion indexes			
Max slope _{infarct}	2.10 ± 0.65	2.23 ± 0.88	4.42 ± 1.82* ^{&}
Max slope _{penumbra}	3.28 ± 1.09	3.34 ± 1.30	5.48 ± 1.62* ^{&}
Max slope _{remote}	5.59 ± 2.18	4.76 ± 2.21	6.49 ± 1.69
Max SI _{infarct}	34.07 ± 17.35	34.02 ± 9.49	40.24 ± 4.95
Max SI _{penumbra}	46.52 ± 14.90	46.02 ± 6.22	49.12 ± 12.76
Max SI _{remote}	55.80 ± 20.51	58.03 ± 13.13	61.60 ± 8.11
TTM _{infarct} , s	17.59 ± 5.44	21.25 ± 6.34	16.24 ± 0.75
TTM _{penumbra} , s	15.93 ± 5.79	19.46 ± 6.24	14.58 ± 0.86
TTM _{remote} , s	14.23 ± 6.13	17.70 ± 5.31	14.20 ± 1.58
CMR LGE indexes			
Infarct size, %	10.42 ± 3.87	8.65 ± 4.47	8.43 ± 4.77
Infarct transmural, %	0 (0 to 49.82)	0 (0 to 46.31)	0 (0 to 27.52)
LGE SI _{infarct}	2505 ± 229.2	2309 ± 231.2	2449 ± 165.4
LGE SI _{penumbra}	2203 ± 168.6	2106 ± 277.6	2312 ± 160.8
LGE SI _{remote}	2062 ± 167.7	1935 ± 234.7	2035 ± 175.1

CTP, CT perfusion; MBF, myocardial blood flow; SI, signal intensity; TTM, time to maximum signal intensity; LGE, late gadolinium enhancement and other abbreviations as in Table 1. *Statistically significant vs. acute setting. [&]Statistically significant vs. sub-acute setting

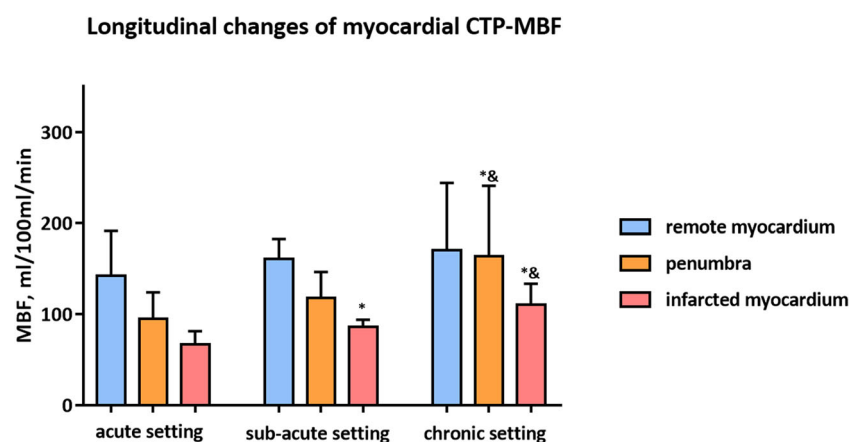
included in the segment analysis. CTP-MBF was positively correlated with the max slope (acute setting: $r = 0.599$, $p < 0.001$; sub-acute setting: $r = 0.627$, $p < 0.001$; chronic setting: $r = 0.680$, $p < 0.001$; all settings: $r = 0.584$, $p < 0.001$) and with the max SI (acute setting: $r = 0.422$, $p < 0.001$; sub-acute setting: $r = 0.309$, $p = 0.021$; chronic setting: $r = 0.567$, $p = 0.002$; all settings: $r = 0.357$, $p < 0.001$), and negatively correlated with the MMT (acute setting: $r = -0.345$, $p = 0.001$; sub-acute setting: $r = -0.436$, $p = 0.001$; chronic setting: $r = -0.587$, $p = 0.020$; all settings: $r = -0.378$, $p < 0.001$) (Table 3). Additionally, CTP-MBF could

differentiate between infarcted segments and non-infarcted segments (area under curve: 0.786, $p < 0.001$) and was associated with infarct transmural per segment ($r = -0.653$, $p < 0.001$) based on LGE (Table 2).

Correlation between CTP-MBF and histologic findings

The area with decreased CTP-MBF coincided with the infarcted area on TTC staining (Fig. 3). The segmental CTP-MBF also showed the ability to identify infarcted segments (area under curve: 0.810, $p < 0.001$) and correlated with infarct

Fig. 1 The changes of CTP-MBF in infarcted myocardium, penumbra, and remote myocardium from the acute to chronic settings. CTP, CT perfusion; MBF, myocardial blood flow. *Statistically significant vs. acute setting. [&]Statistically significant vs. sub-acute setting



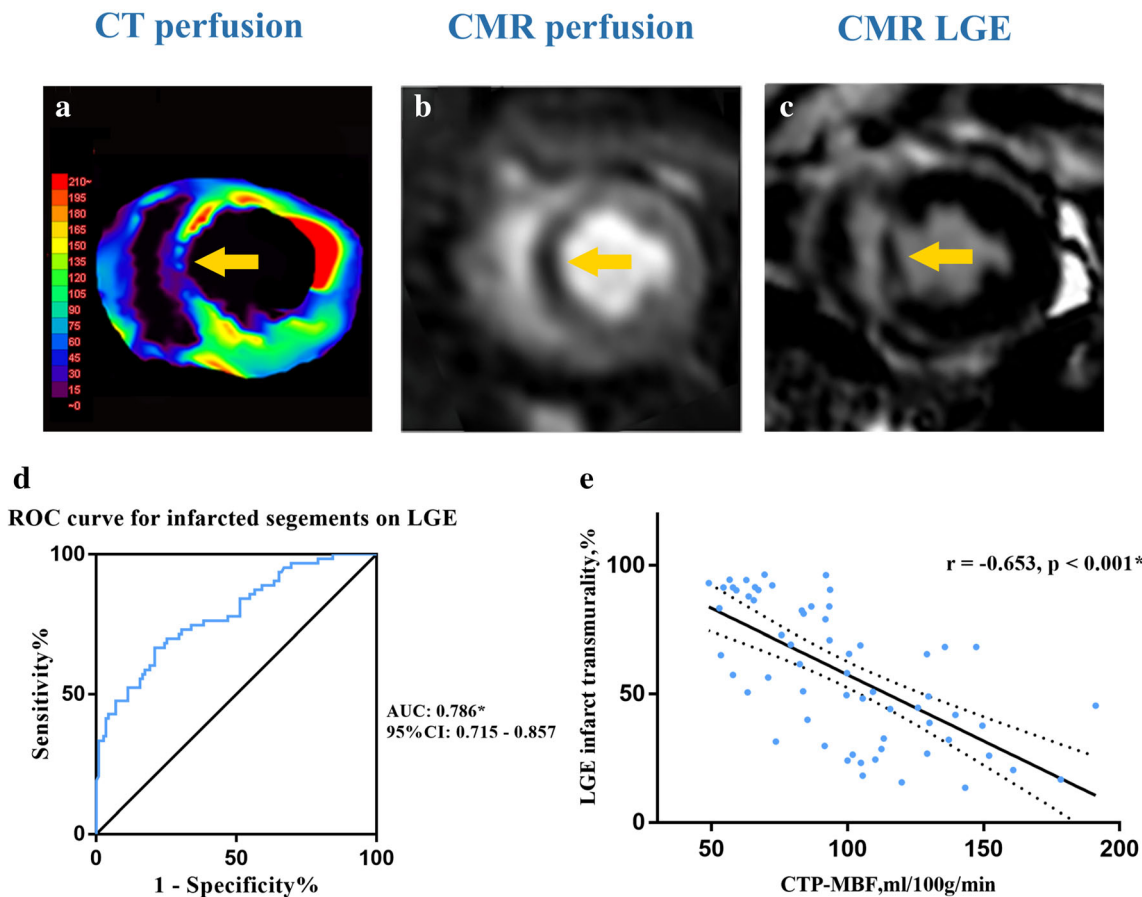


Fig. 2 The CTP-MBF color map and CMR images of one exemplar case. The infarcted myocardium is depicted as the perfusion defect (yellow arrow) on CTP-MBF color map (a) and CMR perfusion (b), and the enhancement (yellow arrow) on CMR LGE (c). **d** Shows the diagnostic performance of

CTP-MBF to identify infarcted segments. **e** Demonstrates the correlation of CTP-MBF with infarct transmuralty on LGE. CMR, cardiac magnetic resonance; LGE, late gadolinium enhancement; ROC, receiver operating characteristic; AUC, area under curve and other abbreviations as in Fig. 1

Table 3 The correlation of CTP-MBF with CMR perfusion indexes

	ROI correlation		Segment correlation	
	<i>R</i>	<i>p</i> value	<i>R</i>	<i>p</i> value
Acute setting				
Max slope	0.787	<i>p</i> < 0.001*	0.599	<i>p</i> < 0.001*
Max SI	0.541	<i>p</i> < 0.001*	0.422	<i>p</i> < 0.001*
TTM	-0.464	<i>p</i> = 0.001*	-0.345	<i>p</i> = 0.001*
Sub-acute setting				
Max slope	0.741	<i>p</i> < 0.001*	0.627	<i>p</i> < 0.001*
Max SI	0.648	<i>p</i> < 0.001*	0.309	<i>p</i> = 0.021*
TTM	-0.412	<i>p</i> = 0.024*	-0.436	<i>p</i> = 0.001*
Chronic setting				
Max slope	0.848	<i>p</i> < 0.001*	0.680	<i>p</i> < 0.001*
Max SI	0.796	<i>p</i> = 0.003*	0.567	<i>p</i> = 0.002*
TTM	-0.604	<i>p</i> = 0.017*	-0.587	<i>p</i> = 0.020*
All settings				
Max slope	0.784	<i>p</i> < 0.001*	0.584	<i>p</i> < 0.001*
Max SI	0.564	<i>p</i> < 0.001*	0.357	<i>p</i> < 0.001*
TTM	-0.417	<i>p</i> < 0.001*	-0.378	<i>p</i> < 0.001*

CTP-MBF, myocardial blood flow derived by CT perfusion; ROI, region of interest and other abbreviations as in Table 2. * *p* value < 0.05, significant

transmuralty per segment ($r = -0.564, p = 0.003$) by TTC staining.

Microscopically, H&E and CD31 staining exhibited myocardial injury and microvessels in various regions of the post-MI myocardium, respectively (Figs. 4 and 5). Similar to the histological variation, CTP-MBF also highlighted the different degrees of microvascular function impairment in infarcted myocardium and penumbra and its recovery during follow-up. The ROI-based CTP-MBF also exhibited a positive correlation with the myocardial microvascular density on CD31 staining ($r = 0.561, p = 0.002$).

Reproducibility of CTP-MBF measurement

The intra-observer and inter-observer variability for ROI measurement of CTP-MBF were 0.962 (95% CI: 0.939 to 0.977) and 0.930 (95% CI: 0.890 to 0.956), respectively. As for segmental measurement of CTP-MBF, the intra-observer and inter-observer variabilities were 0.935 (95% CI: 0.897 to 0.959) and 0.897 (95% CI: 0.856 to 0.915), respectively.

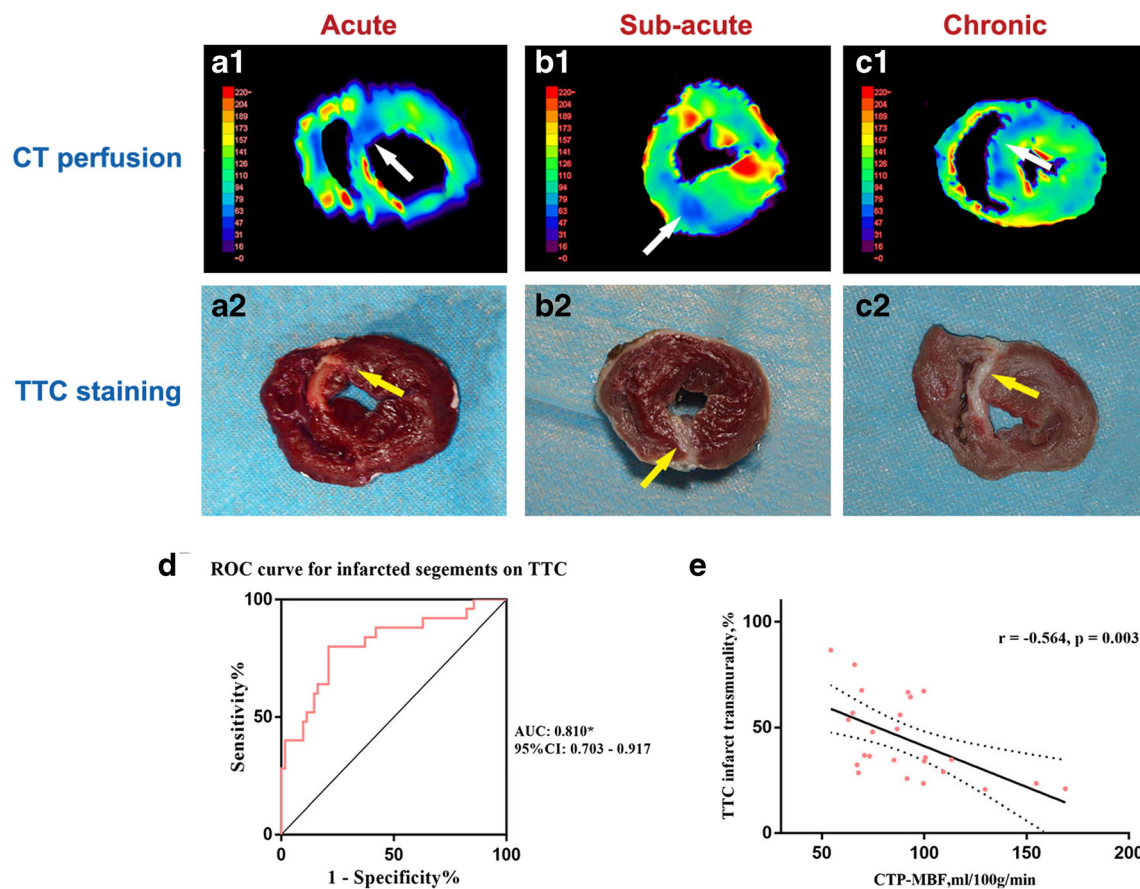


Fig. 3 The CTP-MBF color maps and TTC staining of representative cases in acute (a), sub-acute (b), and chronic (c) setting. The CTP-MBF of infarcted myocardium (white arrow) is evidently decreased on CTP-MBF color maps, and the corresponding area demonstrates the poorly stained area (yellow arrow) on TTC staining. c Shows the diagnostic

performance of CTP-MBF to identify infarcted segments. d Demonstrates the correlation of CTP-MBF with infarct transmural percentage on TTC staining. TTC, triphenyl tetrazolium chloride and other abbreviations as in Fig. 2

Discussion

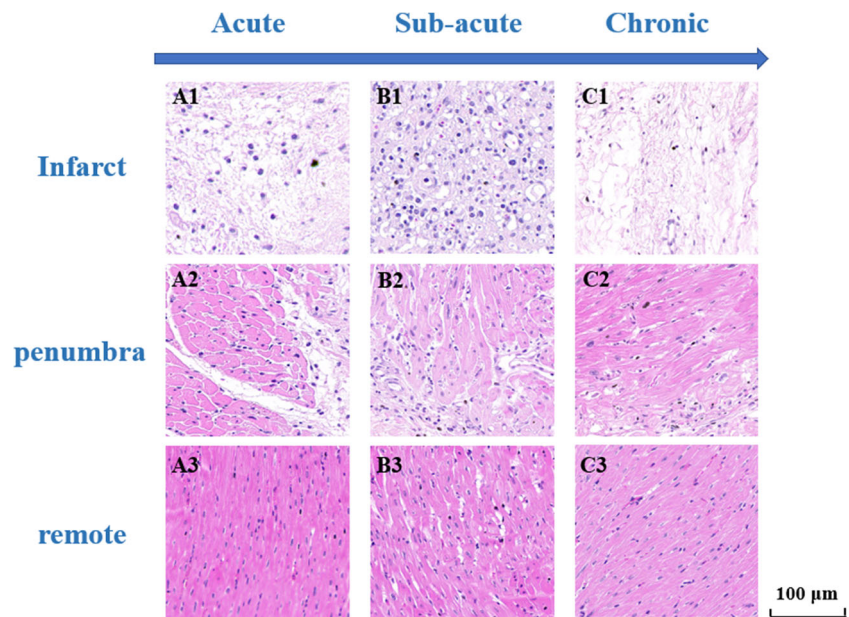
This experimental study investigated the microvascular function of different regions of the post-MI myocardium over time using CTP-MBF. We also evaluated the accuracy of CTP-MBF against contemporary CMR and then conducted histological validation. The main findings of this study are as follows: (1) the microvascular impairment by CTP-MBF was associated with the myocardial injury severity following MI; (2) severe microvascular impairment in acute setting caused poor recovery of the microvascular function during follow-up; (3) CTP-MBF provided a reliable assessment of microvascular function that was subsequently validated by histological findings and in good agreement with the respective CMR indexes. CTP-MBF could be a promising biomarker that facilitates effective risk stratification of patients following MI and enhances treatment efficacy evaluation during follow-up.

The microcirculation following MI plays a key role in myocardial injury healing. More specifically, the assessment of

microvascular function provides an in-depth understanding of the underlying pathophysiological mechanisms and it can evaluate the efficacy of cardioprotective interventions, such as ischemic post-conditioning and N-acetylcysteine with nitrate therapy [3, 28]. With the development of techniques, CTP has become the potential modality for the early risk stratification and long-term follow-up assessment following MI. As previous studies demonstrated, CTP achieved the similar diagnostic value for myocardial ischemia or myocardial infarction when compared with SPECT and MRI [16, 29] and had the distinct advantage of fast acquisition.

Following acute MI, the compromised myocardium may have different degrees of injury and a wide range of myocardial microcirculation [3, 4]. Our results showed the microvascular impairment is closely associated with myocardial injury severity, and CTP-MBF has the capacity to reflect the decreased perfusion gradient from the remote to the infarcted myocardium. Borlotti A et al highlight that microvascular impairment following MI is reversible [3]. The present study also

Fig. 4 H&E staining demonstrates the injury severity of different regions of the post-MI myocardium. The degree of myocardial injury becomes more serious from the remote myocardium to the infarcted one. H&E, hematoxylin-eosin; MI, myocardial infarction

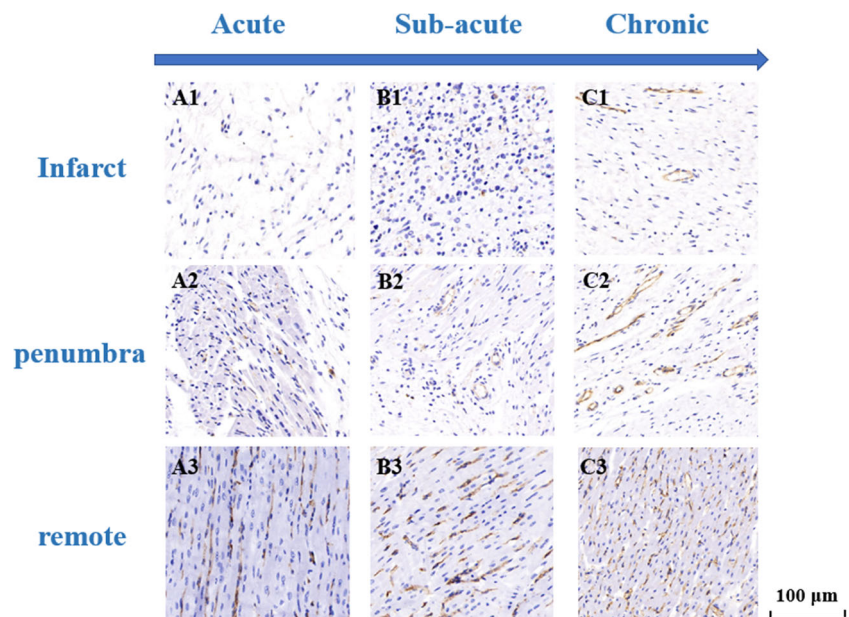


verified the observed increase of CTP-MBF both in the infarcted myocardium and the penumbra during follow-up. Compared with the penumbra, a less pronounced recovery of microvascular function was observed in the infarcted myocardium which underwent more severe microvascular dysfunction in acute settings. Identification of the microvascular impairment severity could facilitate the early stratification of high-risk patients who need to undergo more intensive interventions.

As a widely accepted modality in clinical practice, CMR first-pass perfusion demonstrates the diagnostic accuracy for myocardial ischemia, which was confirmed by coronary

angiography [30, 31]. CMR perfusion is radiation-free and facilitates the quantitative assessment of microvascular function in different cardiac disorders [3, 4, 22, 32]. However, the duration of CMR is relatively long and has the need of multiple breath-hold which is a challenging task in some patients with poor cooperation or in unstable status [20]. CTP could act as a time-saving approach in this situation and its combination of CTA further propels the evaluation of coronary artery anatomy and myocardial perfusion in a one-shot examination [8, 9, 11, 12]. To determine the accuracy of CTP-MBF for quantitative assessment of microvascular function following MI, we explored the correlation of CTP-MBF with

Fig. 5 Immunoreactive CD31 staining shows the microvessels of different regions of the post-MI myocardium. Microvessel formation is observed in both the infarcted myocardium and penumbra during follow-up, and it is more pronounced in the penumbra. Abbreviations are as in Fig. 4



contemporary indexes of CMR perfusion and LGE. Although several previous studies have already performed a comparison between CTP-MBF and CMR [16, 18], they have mainly focused on the diagnostic efficiency of CTP-MBF to detect the manifested abnormality on CMR. The present study further demonstrates a good agreement between CTP-MBF and CMR regarding the infarct extent and the ischemic severity.

Several published studies have shown that quantitative CTP is a sensitive tool for myocardial perfusion [33] and could distinguish myocardial ischemia both in the ex vivo and in vivo CAD animal models [34–39], which achieved good correlation with microsphere perfusion [36–39]. However, the histology examination was not conducted, possibly for the reason that myocardial damage was not severe in transiently induced CAD models. As for MI models, the previous studies measured the changes of CTP-MBF in infarcted and normal myocardium over time and showed the approximate coincidence of CTP-MBF decreased area with the infarcted zone on TTC staining [40, 41]. Based on these findings, our study further explored the change of CTP-MBF in different myocardial regions (including penumbra) following MI in a longer period. The results demonstrated the diagnostic performance of CTP for myocardial viability on TTC staining. More importantly, the variation of CTP-MBF was consistent with the microscopical findings of CD31 staining, indicating the ability of CTP-MBF to quantify microvascular function impairments and reflect its recovery during follow-up.

Continuous advances in technology have led to a growing usage of CTP in clinical practice. Different strategies and post-processing are introduced to reduce the radiation dose during the examination and to improve image quality for perfusion analysis [42–44]. However, it should be acknowledged that heterogeneity in various tracer kinetic models for MBF still requires attentions [45]. Future exploration is needed to compare the respective robustness of different models and to establish the standard reference for normal perfusion based on large databases.

Our study also had several limitations. First, the differences in the CTP-MBF absolute value can be expected for different vendors, scan protocols, and post-processing software. Although this is a proof-of-concept study for microvascular function assessment using CTP-MBF, a suitable and well-defined reference standard for CTP-MBF should be established in future clinical studies. Secondly, stress perfusion was not performed. It may provide more appropriate indicators of microvascular function and obstruction. Thirdly, this was an animal study with ideal laboratory settings; clinical results may vary. But our findings provided experimental evidence for clinical studies. Finally, the fully quantitative MR perfusion method was recently developed to assess MBF, but it was not implemented in this experimental setting [46]. The application of this technique in MI needs to be further investigated in future studies.

In conclusion, CTP-MBF allows the quantitative assessment of the microvascular function after MI and demonstrates the capacity to track its variations over time. Moreover, CTP-MBF shows good agreement with contemporary CMR and histologic findings. Thus, the present study provides experimental evidence for the effective application of CTP-MBF in microvascular function evaluation following MI. Further clinical studies should be performed in order to verify our findings.

Funding This work was supported by the National Natural Science Foundation of China (81471721, 81471722, 81641169, 81771887, 81771897, 81901712, and 81971586); the Program for New Century Excellent Talents in University (No. NCET-13-0386); the Program for Young Scholars and Innovative Research Team in Sichuan Province (No. 2017TD0005) of China; the Applied and Fundamental Study of Sichuan Province (No. 2017JY0026); and 1·3·5 project for disciplines of excellence, West China Hospital, Sichuan University (No. ZYGD18013).

Compliance with ethical standards

Guarantor The scientific guarantor of this publication is Zhi-gang Yang.

Conflict of interest One of the authors of this manuscript (Xiao-yue Zhou) is an employee of Siemens Healthcare. The remaining authors declare no relationships with any companies whose products or services may be related to the subject matter of the article.

Statistics and biometry No complex statistical methods were necessary for this paper.

Informed consent Approval from the institutional animal care committee was obtained.

Ethical approval Institutional Review Board approval was obtained.

Methodology

- prospective
- experimental
- performed at one institution

References

1. Symons R, Pontone G, Schwitter J et al (2018) Long-term incremental prognostic value of cardiovascular magnetic resonance after ST-segment elevation myocardial infarction: a study of the collaborative registry on CMR in STEMI. *JACC Cardiovasc Imaging* 11(6):813–825
2. de Waha S, Patel MR, Granger CB et al (2017) Relationship between microvascular obstruction and adverse events following primary percutaneous coronary intervention for ST-segment elevation myocardial infarction: an individual patient data pooled analysis from seven randomized trials. *Eur Heart J* 38(47):3502–3510
3. Borlotti A, Jerosch-Herold M, Liu D et al (2019) Acute microvascular impairment post-reperused STEMI is reversible and has additional clinical predictive value: A CMR OXAMI Study. *JACC Cardiovasc Imaging* 12(9):1783–1793
4. Bethke A, Shanmuganathan L, Andersen GØ et al (2019) Microvascular perfusion in infarcted and remote myocardium after

- successful primary PCI: angiographic and CMR findings. *Eur Radiol* 29(2):941–950
5. Danad I, Szymonifka J, Twisk JWR et al (2017) Diagnostic performance of cardiac imaging methods to diagnose ischaemia-causing coronary artery disease when directly compared with fractional flow reserve as a reference standard: a meta-analysis. *Eur Heart J* 38(13):991–998
 6. Gupta A, Taqueti VR, van de Hoef TP et al (2017) Integrated noninvasive physiological assessment of coronary circulatory function and impact on cardiovascular mortality in patients with stable coronary artery disease. *Circulation* 136(24):2325–2336
 7. Gould KL, Johnson NP, Roby AE et al (2019) Regional, artery-specific thresholds of quantitative myocardial perfusion by PET associated with reduced myocardial infarction and death after revascularization in stable coronary artery disease. *J Nucl Med* 60(3):410–417
 8. Danad I, Szymonifka J, Schulman-Marcus J, Min JK (2016) Static and dynamic assessment of myocardial perfusion by computed tomography. *Eur Heart J Cardiovasc Imaging* 17(8):836–844
 9. Takx RAP, Celeng C, Schoepf UJ (2018) CT myocardial perfusion imaging: ready for prime time? *Eur Radiol* 28(3):1253–1256
 10. Feger S, Rief M, Zimmermann E et al (2015) Patient satisfaction with coronary CT angiography, myocardial CT perfusion, myocardial perfusion MRI, SPECT myocardial perfusion imaging and conventional coronary angiography. *Eur Radiol* 25(7):2115–2124
 11. Pursnani A, Lee AM, Mayrhofer T et al (2015) Early resting myocardial computed tomography perfusion for the detection of acute coronary syndrome in patients with coronary artery disease. *Circ Cardiovasc Imaging* 8(3):e002404. <https://doi.org/10.1161/CIRCIMAGING.114.002404>
 12. Pontone G, Andreini D, Guaricci AI et al (2018) Quantitative vs. qualitative evaluation of static stress computed tomography perfusion to detect haemodynamically significant coronary artery disease. *Eur Heart J Cardiovasc Imaging* 19(11):1244–1252
 13. Nakamura S, Kitagawa K, Goto Y et al (2019) Incremental prognostic value of myocardial blood flow quantified with stress dynamic computed tomography perfusion imaging. *JACC Cardiovasc Imaging* 12(7 Pt 2):1379–1387
 14. Chen MY, Rochitte CE, Arbab-Zadeh A et al (2017) Prognostic value of combined CT angiography and myocardial perfusion imaging versus invasive coronary angiography and nuclear stress perfusion imaging in the prediction of major adverse cardiovascular events: the CORE320 multicenter study. *Radiology* 284(1):55–65
 15. Van Rosendael AR, Dimitriu-Leen AC, de Graaf MA et al (2017) Impact of computed tomography myocardial perfusion following computed tomography coronary angiography on downstream referral for invasive coronary angiography, revascularization and, outcome at 12 months. *Eur Heart J Cardiovasc Imaging* 18(9):969–977
 16. Tanabe Y, Kido T, Uetani T et al (2016) Differentiation of myocardial ischemia and infarction assessed by dynamic computed tomography perfusion imaging and comparison with cardiac magnetic resonance and single-photon emission computed tomography. *Eur Radiol* 26(11):3790–3801
 17. Yim NY, Kim YH, Choi S et al (2009) Multidetector-row computed tomographic evaluation of myocardial perfusion in re-perfused chronic myocardial infarction: value of color-coded perfusion map in a porcine model. *Int J Cardiovasc Imaging* 25(Suppl 1):65–74
 18. Bamberg F, Marcus RP, Becker A et al (2014) Dynamic myocardial CT perfusion imaging for evaluation of myocardial ischemia as determined by MR imaging. *JACC Cardiovasc Imaging* 7(3):267–277
 19. Kidambi A, Motwani M, Uddin A et al (2017) Myocardial extracellular volume estimation by CMR predicts functional recovery following acute MI. *JACC Cardiovasc Imaging* 10(9):989–999
 20. Liu D, Borlotti A, Viliani D et al (2017) CMR Native T1 Mapping allows differentiation of reversible versus irreversible myocardial damage in ST-segment-elevation myocardial infarction: an OxAMI study (Oxford Acute Myocardial Infarction). *Circ Cardiovasc Imaging* 10(8):e005986. <https://doi.org/10.1161/CIRCIMAGING.116.005986>
 21. Eitel I, Pöss J, Jobs A et al (2015) Left ventricular global function index assessed by cardiovascular magnetic resonance for the prediction of cardiovascular events in ST-elevation myocardial infarction. *J Cardiovasc Magn Reson* 17:62
 22. Li R, Yang ZG, Wen LY et al (2016) Regional myocardial microvascular dysfunction in cardiac amyloid light-chain amyloidosis: assessment with 3 T cardiovascular magnetic resonance. *J Cardiovasc Magn Reson* 18:16
 23. van Assen M, Lavra F, Schoepf UJ et al (2019) Iodine quantification based on rest/stress perfusion dual energy CT to differentiate ischemic, infarcted and normal myocardium. *Eur J Radiol* 112:136–143
 24. Krumm P, Martirosian P, Rath D et al (2016) Signal decay mapping of myocardial edema using dual-contrast fast spin-echo MRI. *J Magn Reson Imaging* 44(1):186–193
 25. Robbers LF, Delewi R, Nijveldt R et al (2013) Myocardial infarct heterogeneity assessment by late gadolinium enhancement cardiovascular magnetic resonance imaging shows predictive value for ventricular arrhythmia development after acute myocardial infarction. *Eur Heart J Cardiovasc Imaging* 14(12):1150–1158
 26. Zou J, Fei Q, Xiao H et al (2019) VEGF-A promotes angiogenesis after acute myocardial infarction through increasing ROS production and enhancing ER stress-mediated autophagy. *J Cell Physiol* 234(10):17690–17703
 27. Robbers LF, Eerenberg ES, Teunissen PF et al (2013) Magnetic resonance imaging-defined areas of microvascular obstruction after acute myocardial infarction represent microvascular destruction and haemorrhage. *Eur Heart J* 34(30):2346–2353
 28. Bulluck H, Chan MHH, Paradies V et al (2018) Impact of cardioprotective therapies on the edema-based area at risk by CMR in reperfused STEMI. *J Am Coll Cardiol* 71(24):2856–2858
 29. Meinel FG, De Cecco CN, Schoepf UJ et al (2014) First-arterial-pass dual-energy CT for assessment of myocardial blood supply: do we need rest, stress, and delayed acquisition? Comparison with SPECT. *Radiology* 270(3):708–716
 30. Vincenti G, Masci PG, Monney P et al (2017) Stress perfusion CMR in patients with known and suspected CAD: prognostic value and optimal ischemic threshold for revascularization. *JACC Cardiovasc Imaging* 10(5):526–537
 31. Cheng AS, Pegg TJ, Karamitsos TD et al (2007) Cardiovascular magnetic resonance perfusion imaging at 3-tesla for the detection of coronary artery disease: a comparison with 1.5-tesla. *J Am Coll Cardiol* 49(25):2440–2449
 32. Chiribiri A, Leuzzi S, Conte MR et al (2015) Rest perfusion abnormalities in hypertrophic cardiomyopathy: correlation with myocardial fibrosis and risk factors for sudden cardiac death. *Clin Radiol* 70(5):495–501
 33. Scherer K, Hammel J, Sellerer T et al (2019) Dynamic quantitative iodine myocardial perfusion imaging with dual-layer CT using a porcine model. *Sci Rep* 9(1):16046
 34. Poulter R, Wood DA, Starovoytov A, Smith S, Chitsaz M, Mayo J (2019) Development of a porcine model of coronary stenosis using fully percutaneous techniques suitable for performing cardiac computed tomography, CT-perfusion imaging and fractional flow reserve. *Heart Lung Circ* 28(8):1292–1300
 35. Pelgrim GJ, Duguay TM, Stijnen JM et al (2017) Analysis of myocardial perfusion parameters in an ex-vivo porcine heart model using third generation dual-source CT. *J Cardiovasc Comput Tomogr* 11(2):141–147
 36. Pelgrim GJ, Das M, van Tuijl S et al (2017) Validation of myocardial perfusion quantification by dynamic CT in an ex-vivo porcine heart model. *Int J Cardiovasc Imaging* 33(11):1821–1830

37. Hubbard L, Lipinski J, Ziemer B et al (2018) Comprehensive assessment of coronary artery disease by using first-pass analysis dynamic CT Perfusion: validation in a swine model. *Radiology* 286(1):93–102
38. George RT, Jerosch-Herold M, Silva C et al (2007) Quantification of myocardial perfusion using dynamic 64-detector computed tomography. *Invest Radiol* 42(12):815–822
39. Bamberg F, Hinkel R, Schwarz F et al (2012) Accuracy of dynamic computed tomography adenosine stress myocardial perfusion imaging in estimating myocardial blood flow at various degrees of coronary artery stenosis using a porcine animal model. *Invest Radiol* 47(1):71–77
40. So A, Wisenberg G, Teefy P et al (2018) Functional CT assessment of extravascular contrast distribution volume and myocardial perfusion in acute myocardial infarction. *Int J Cardiol* 266:15–23
41. So A, Hsieh J, Li JY, Hadway J, Kong HF, Lee TY (2012) Quantitative myocardial perfusion measurement using CT perfusion: a validation study in a porcine model of reperfused acute myocardial infarction. *Int J Cardiovasc Imaging* 28(5):1237–1248
42. Levi J, Eck BL, Fahmi R et al (2019) Calibration-free beam hardening correction for myocardial perfusion imaging using CT. *Med Phys* 46(4):1648–1662
43. Li Y, Speidel MA, Francois CJ, Chen GH (2017) Radiation dose reduction in CT myocardial perfusion imaging using SMART-RECON. *IEEE Trans Med Imaging* 36(12):2557–2568
44. Gong C, Han C, Gan G et al (2017) Low-dose dynamic myocardial perfusion CT image reconstruction using pre-contrast normal-dose CT scan induced structure tensor total variation regularization. *Phys Med Biol* 62(7):2612–2635
45. van Assen M, Pelgrim GJ, De Cecco CN et al (2019) Intermodel disagreement of myocardial blood flow estimation from dynamic CT perfusion imaging. *Eur J Radiol* 110:175–180
46. Engblom H, Xue H, Akil S et al (2017) Fully quantitative cardiovascular magnetic resonance myocardial perfusion ready for clinical use: a comparison between cardiovascular magnetic resonance imaging and positron emission tomography. *J Cardiovasc Magn Reson* 19(1):78

Publisher's note Springer Nature remains neutral with regard to jurisdictional claims in published maps and institutional affiliations.